JACS
JOURNAL OF THE AMERICAN CHEMICAL SOCIETY
pubs.acs.org/JACS
Communication

Atomically Conformal Metal Laminations on Plasmonic Nanocrystals for Efficient Catalysis

Anubhab Acharya, Sateesh Dubbu, Sumit Kumar, Nitee Kumari, Yeseul Kim, Sunae So, Taewan Kwon, Zhipeng Wang, Junbeom Park, Yoon-Kyoung Cho, Junsuk Rho, Sang Ho Oh, Amit Kumar,* and In Su Lee*

Cite This: J. Am. Chem. Soc. 2021, 143, 10582−10589

ABSTRACT: Despite the enormous application potential, methods for conformal few-atomic-layer deposition on colloidal nanocrystals (NCs) are scarce. Similar to the process of lamination, we introduce a "confine and shine" strategy to homogeneously modify the different surface curvatures of plasmonic NCs with ultrathin conformal layers of diverse catalytic noble metals. This self-limited epitaxial skinlike metal growth harvests the localized surface plasmon resonance to induce reduction chemistry directly on the NC surface, confined inside hollow silica. This strategy avoids any kinetic anisotropic metal deposition. Unlike the conventional thick, anisotropic, and dendritic shells, which show severe nonradiative damping, the skinlike metal lamination preserves the key plasmonic properties of the core NCs. Consequently, the plasmonic−catalytic hybrid nanoreactors can carry out a variety of organic reactions with impressive rates.

Tailoring the surfaces of metal nanocrystals (NCs) can tap into the wealth of unique physical and chemical properties.[1] Bimetallic core@shell NCs have attracted immense interest because they can harness interfacial synergy from the core and shell counterparts, rendering applications in catalysis, plasmonics, electronics, displays, and magnetics.[2] The continuous skinlike atomic layers have several advantages such as maximization of the surface atomic utilization efficiency, interfacial lattice effects, light-induced energy transfer processes, and surface-protective effects.[3] Combining plasmonic NCs (e.g., Au, Ag, Cu) with noble transition metals (e.g., Pt, Pd, Rh, Ru) results in "antenna−reactor" hybrid systems for efficient localized surface plasmon resonance (LSPR)-driven catalysis.[4] However, it is critical to limit the thickness of the nonplasmonic light-absorbing dielectric shell to preserve the characteristic LSPR extinction and efficient electromagnetic energy funneling on the whole NC surface.[4c] Normally, kinetic metal growth results in spatial anisotropies in growing metal shells, forming dendrites, islands, or grains.[5] This is due to several factors such as differential reactivities of crystalline facets, lattice mismatch/strain, differences in atomic cohesive energies, the presence of multiple nucleation sites, and variable densities of surface ligands. Conventional strategies using high temperatures, metal etching, underpotential deposition, and so on can reshape, deform, overgrow, or sinter the NCs, compromising their hallmark plasmonic characteristics.[6] Despite the enormous applied potential, there is no generalized method to apply diverse atomically thin conformal metal coatings on different core shapes. We envisioned using LSPR-induced surface-localized energy transfer to direct the atomic growth selectively on the NC surface.[7] The key challenges in developing such a colloidal synthetic strategy were (i) to create a ligand-free confined environment on the core NCs to eliminate any kinetics-directing role[8] and (ii) to localize the plasmonic effect on individually isolated NCs by restricting their interparticle interactions, thereby avoiding any nonspecific reactions.[4] Here we introduce the "confine and shine" strategy to homogeneously laminate the different surface curvatures of plasmonic NCs (e.g., rod, sphere, cube, trigonal bipyramid, and dodecahedron) with ultrathin conformal layers (<1 nm) of diverse catalytic noble metals (e.g., Pt, Pd, Ru, and Rh) (Scheme 1). We apply LSP-resonant laser irradiation to activate self-limited photochemical metal reduction chemistry directly on the plasmonic NC inside hollow silica. This approach utilizes highly localized plasmonic energy on individually isolated NCs without any undesired increase in bulk solution reaction rates. In addition, the isolated NC surface in combination with laser-induced effects can effectively overcome the anisotropic metal growth. Because the metallic lamination is ultrathin, the hallmark plasmonic properties of the NCs remain well-preserved, and the resulting plasmonic−catalytic nanoreactors carry out a variety of chemical transformations with high photoconversion efficiencies and turnover frequencies (TOFs). The current methodology embarks upon the use of light energy and LSPR-induced chemistry for nanostructure surface manipulation, resulting in enhanced properties and diverse applications.

To implement our "confine and shine" strategy, we chose gold nanorods (AuNRs) as typical plasmonic NCs.[9] Because of

Received: June 6, 2021
Published: July 2, 2021

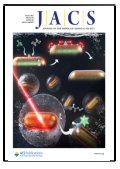

https://doi.org/10.1021/jacs.1c05753
J. Am. Chem. Soc. 2021, 143, 10582−10589

Scheme 1. "Confine and Shine" Strategy for [M] Lamination on Plasmonic NCs

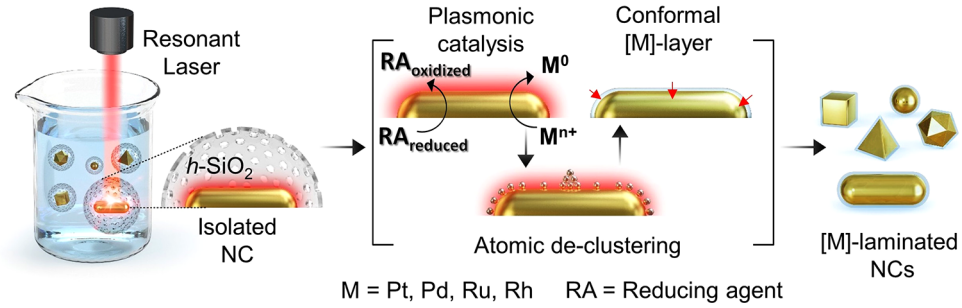

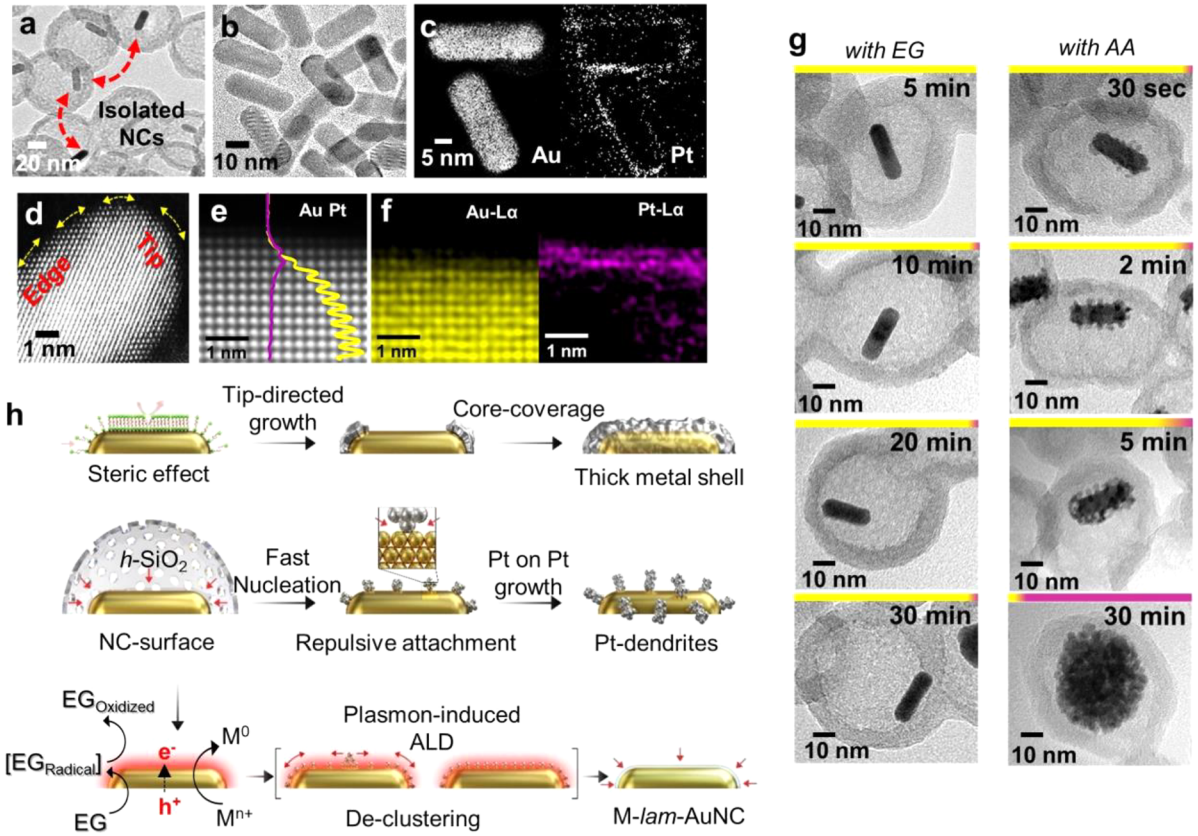

Figure 1. (a) TEM image of Pt-laminated AuNRs in hollow silica (**Pt-*lam*-AuNR**@*h*SiO_2). (b) TEM image of **Pt-*lam*-AuNR** after silica removal. (c) EELS elemental mapping of **Pt-*lam*-AuNRs**. (d, e) HAADF-STEM images of a **Pt-*lam*-AuNR**. (f) EDS elemental mapping and line profile for a **Pt-*lam*-AuNR**. (g) Comparative time-course TEM images of Pt growth with ethylene glycol (EG) and ascorbic acid (AA) under laser irradiation (785 nm, 0.4 W/cm^2). Yellow and pink color gradient bars on each TEM image represent the relative atomic percentages of Au (yellow) and Pt (pink) as measured by EDS. (h) Schematic of the metal growth mechanisms on CTAB-AuNRs and AuNR@*h*-SiO_2 with strong reducing agents and plasmon-induced photocatalytic atomic layer deposition (ALD) using EG. $EG_{Oxidized}$ and $EG_{Radical}$ represent the oxidized and radical forms of EG, respectively. M^{n+} and M^0 are the starting and reduced forms of the metal precursor. h^+ and e^- are the plasmonic charge carriers participating in the redox reactions.

the presence of curves (on the tips) and flat surfaces (on the edges) having different crystal facets and varying ligand densities as well as the repulsive interaction between Pt and Au, AuNRs are challenging to modify with a homogeneous thin conformal Pt layer—rather, Pt-on-Pt anisotropic clustering usually occurs.[5] First, to access the individually isolated AuNRs, we synthesized rattlelike hollow structures having only a single AuNR (aspect ratio 2.7 ± 0.3) surrounded by a hollow silica shell (ca. 80 nm) (denoted as AuNR@*h*-SiO_2) and confirmed the removal of surface ligands during the silica-coating-hollowing process by Fourier transform infrared spectroscopy (FTIR) (Figure S1).[10] Next, a dispersion of AuNR@*h*-SiO_2 (1 mg/mL) and Na_2PtCl_4 (0.5 mL, 50 mM) in ethylene glycol (EG) (10 mL) was exposed to near-infrared (NIR) laser irradiation (0.4 W/cm^2) at the ambient bulk solution temperature (35 °C). Transmission electron microscopy (TEM) of the resulting Pt-laminated AuNRs (**Pt-*lam*-AuNRs**) revealed a slight increase (<1 nm) in the overall size of the original AuNRs due to the conformal Pt deposition (ca. two or three Pt atomic layers) without any measurable change in the aspect ratio (Figure 1a,b and Table S1). Electron energy loss spectroscopy (EELS)-based Au/Pt mapping verified the peripheral Pt atomic layers around the AuNRs (Figure 1c). High-resolution TEM (HRTEM) and high-angle annular dark-

https://doi.org/10.1021/jacs.1c05753
J. Am. Chem. Soc. 2021, 143, 10582−10589

field scanning TEM (HAADF-STEM) affirmed the nanorods to be monocrystalline, devoid of any newly emerged grain boundary or anisotropy on either flat or curved surfaces (Figure 1d,e). Atomic-level-resolved STEM-based energy-dispersive X-ray spectroscopy (STEM-EDS) elemental mapping and line profiling confirmed atomically conformal epitaxial arrangement of Pt atoms stacked on Au atoms (Figure 1f). In addition, X-ray diffraction (XRD) and X-ray photoelectron spectroscopy (XPS) confirmed the chemical species in **Pt-*lam*-AuNRs** (Figures S2 and S3). The XPS Pt 4f peaks of the **Pt-*lam*-AuNRs** showed a decrease in binding energy (ΔE = 0.73 eV) compared with a thicker Pt shell (ca. 3 nm) on AuNRs (Pt-*shell*-AuNRs), indicating facile charge transfer between Au and a larger fraction of Pt in the former case.[11] The presence of a thin Pt skin was also verified after the Au cores were etched away from Pt-*shell*-AuNRs (Figure S4). Oxygen-free conditions did not influence the Pt lamination, ruling out the indirect oxidative activation of EG by in situ-produced singlet oxygen (Figure S5).[12] Also, Pt lamination did not proceed in deionized water (DI) in place of EG, indicating that there was no direct laser-induced reduction of Pt(II) on AuNRs (Figure S6).[13] Moreover, the use of a stronger reducing agent such as ascorbic acid, hydrazine, or hydroxylamine resulted in conventional branched or dendritic excess growth of Pt around the AuNRs (Figures 1g and S7).[5] In a comparative TEM time-course study with ascorbic acid, dendritic Pt growth started at a very early stage (within 1 min) and filled the whole interior volume of *h*-SiO_2, showing similar results in the presence or absence of laser irradiation (Figures 1g and S8). In contrast, with EG no such excess growth of Pt was observed, resulting only in **Pt-*lam*-AuNRs** (~5 atom % Pt, analyzed for 100 particles by EDS) in 30 min, even when higher amounts of Pt precursors were used, indicating the self-limiting nature of the Pt growth (Figure S9). Also, Pt lamination did not proceed without laser irradiation at room temperature (Figure S10). The use of conventional thermal conditions (bulk solution temperature of 50−90 °C) or high laser fluxes (>1.0 W/cm^2) resulted in granular Pt spilled all over the AuNR@*h*-SiO_2 as a result of nonspecific thermal polyol reduction (Figures S11 and S12).[14] The strong reductants largely conducted seed-mediated self-catalytic Pt-on-Pt fast kinetic metal growth, depending on the supply of the Pt precursor and the reaction time. Distinctly, LSPR-induced EG-mediated Pt lamination is highly localized and self-limited only to the availability of bare Au surface. We conducted electron spin resonance (ESR)-based studies, which evidenced the presence of EG radicals upon laser irradiation of a solution of AuNR@*h*-SiO_2 in EG (details are provided in SI section 2.20 and Figure S13). Also, in an FTIR-based study, we identified an oxidized aldehyde form of EG produced upon laser irradiation in the presence of AuNR@*h*-SiO_2 (Figure S14). In contrast, the solution of **Pt-*lam*-AuNR**@*h*-SiO_2 in EG after laser irradiation showed a very weak ESR response (Figure S13). These results suggested that Pt lamination on AuNRs is accompanied by LSPR-induced photocatalytic oxidation of EG through a radical intermediate and is self-limited after full occupation of the Au surface with a few Pt atomic layers. Replacing EG with more reactive hole acceptors such as ethanol and isopropanol resulted granular Pt growth (Figure S15).[14−16] However, other polyols such as diethylene glycol and triethylene glycol acted similar to EG (Figure S16). A photothermal heat flux simulation using COMSOL software (details are provided in SI section 2.29) estimated a very low photothermal increase in the surface temperatures (ΔT = 16.32 and 14.23 K for AuNRs and **Pt-*lam*-AuNRs**, respectively) under continuous-wave (CW) laser irradiation at mild power (Figure S17), which is unlikely to induce any thermal polyol reduction. Replacing the NIR laser (LSPR-resonant) with a blue laser (352 nm) resulted in the formation of a bumpy Pt layer on the AuNRs (ca. 12 wt % Pt), indicating the possibility of utilizing interband transitions for Pt photodeposition (Figure S18).[17] Overall, these results suggested the dominant LSPR-induced photochemical pathway for Pt deposition in the presence of EG. LSPR-induced surface-charge/field redistribution may not only induce surface-selective photocatalytic Pt deposition but also assist in conformal organization of the Pt atoms while avoiding Pt overgrowth and clustering.[18]

To gain insight into the origin of the uniform conformal nature of the Pt layer, we synthesized tiny Pt grains directly interfaced with the AuNRs and irradiated the nanoparticles (NPs) with the NIR laser (details are provided in SI section 2.25 and Figures S19 and S20). A time-course study based on HRTEM and HAADF-STEM revealed the deformation and fusion of Pt grains on the Au surface to form a uniform Pt layer (Figure S20). This suggested a possible contribution of laser-induced declustering of Pt atoms during EG-mediated photochemical deposition of few-layer Pt. In **Pt-*lam*-AuNR**@*h*-SiO_2, there was no structural reorganization of the presynthesized Pt layer into clusters after laser treatment (Figure S21), indicating the high stability of the Au−Pt interfacial structure.[19] When we attempted Pt lamination on cetyltrimethylammonium bromide (CTAB)-coated AuNRs (CTAB-AuNRs) dispersed in EG, severe aggregation of the AuNRs was noticed (Figure S22), and Pt growth was found to originate at the tips because of the lower ligand density, followed by granular growth along the edges (Figure S23).[5] In AuNR@*h*-SiO_2, the ligand-free surface helped to overcome any ligand-induced anisotropic/clusterlike metal growth (Figure S24). Apart from ensuring colloidal stability of the bare AuNRs, optically transparent *h*-SiO_2 kept individual AuNRs isolated from each other to avoid any interparticle plasmonic coupling and NC fusion/welding upon laser irradiation (Figure S25).[20]

Next, we generalized our metal lamination strategy by conducting the growth of other extensively useful catalytic metals (M = Pd, Ru, Rh) on AuNR@*h*-SiO_2 using the Na_2PdCl_4/EG, $RuCl_3$/formaldehyde, and $RhCl_3$/hydroquinone (metal precursor/reducing agent), respectively, resulting in different ultrathin conformal M laminations on AuNRs (Figures S26 and S27). In the latter two cases, stronger reducing agents were necessary because of the lower redox potentials of Ru (E°_{redox} = 0.46 V vs NHE) and Rh (E°_{redox} = 0.76 V vs NHE).[21] Furthermore, we extended the "confine and shine" strategy to other plasmonic NC shapes such as Au spheres, cubes, trigonal bipyramids, and dodecahedra individually located inside *h*-SiO_2 using a resonant green laser (532 nm, 32 mW/cm^2) (Figure S28). When a mixture of AuNR@*h*-SiO_2 and other plasmonic NC shapes (AuNC@*h*-SiO_2) was subjected to Pt lamination using an NIR laser, Pt growth took place only on the AuNRs, with no reaction on other AuNC shapes (Figure S29). Such selective resonant-wavelength-dependent M lamination chemistry validated the crucial LSPR-mediated activation mechanism.

We recorded UV−vis absorption spectra of **Pt-*lam*-AuNR**@*h*-SiO_2, which showed that the absorption at 785 nm is still

https://doi.org/10.1021/jacs.1c05753
J. Am. Chem. Soc. 2021, 143, 10582−10589

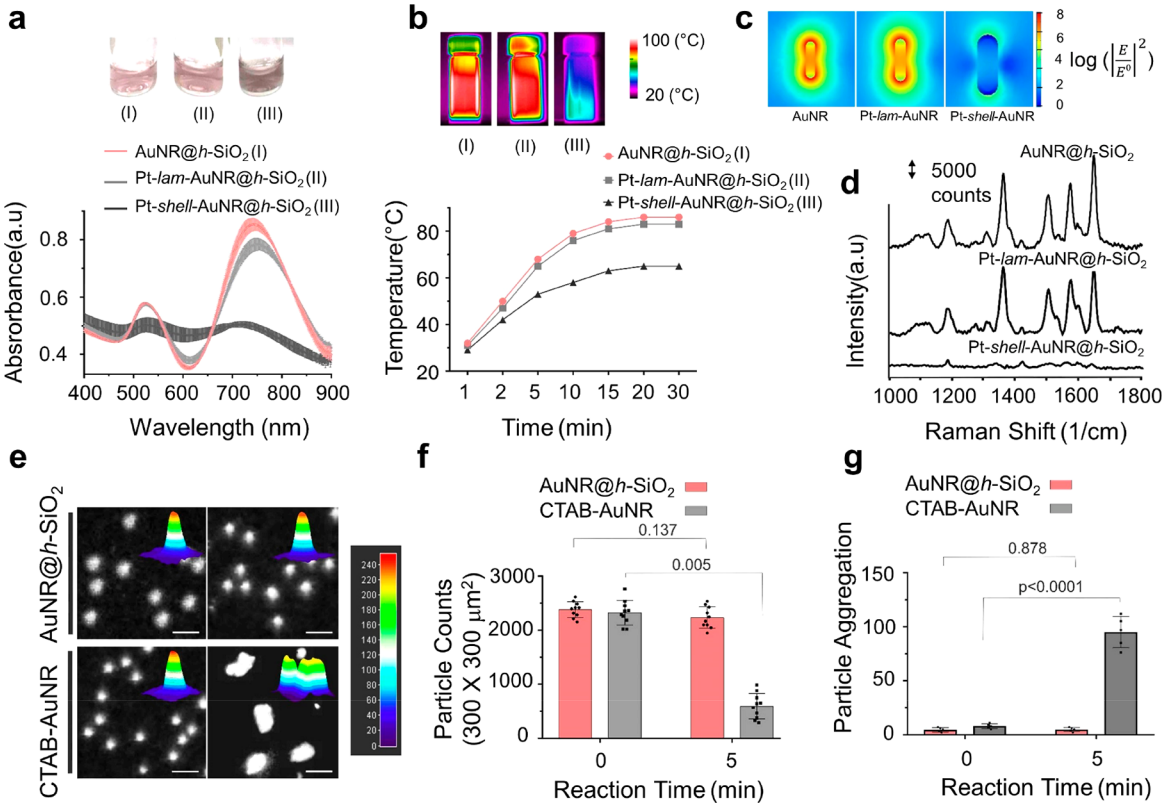

Figure 2. Characterized and simulated plasmonic properties of AuNRs, **Pt-*lam*-AuNRs**, and Pt-*shell*-AuNRs. (a) Digital photographs and UV−vis spectra. (b) IR camera images and photothermal conversions with an NIR laser (785 nm, 2 W/cm^2). (c) Simulated electric field distributions based on finite-element method (FEM) and (d) SERS spectra of Rh6G modified on NC surfaces. (e) Representative dark-field microscopy images: (top) AuNR@*h*-SiO_2 before (left) and after (right) Pt lamination; (bottom) CTAB-AuNRs before (left) and after (right) dispersion in EG. The insets show light intensity profiles on single spots. (f, g) Quantification of bright spots and particle aggregation through dark-field microscopy in each case (details are provided in SI section 2.17).

much stronger than the absorption at 532 nm, with only a slight broadening and suppression of the characteristic longitudinal LSPR absorption due to the minimal change in the dielectric environment resulting from the ultrathin Pt atomic layer (Figure 2a).[5] However, in the case of a thicker Pt shell (Pt-*shell*-AuNR@*h*-SiO_2), the LSPR band at 785 nm was suppressed dramatically, indicating poor absorption in the NIR region. Also, the photothermal conversions by **Pt-*lam*-AuNR@***h*-SiO_2 and AuNR@*h*-SiO_2 were similar ($\Delta T \approx 32$ °C with 785 nm laser irradiation at 2 W/cm^2) (Figures 2b and S30). Surface-enhanced Raman scattering (SERS) was also found to be highly sensitive to the LSPR properties: the characteristic peak intensities of rhodamine 6G modified on AuNR@*h*-SiO_2 and **Pt-*lam*-AuNR** were comparable, but that on Pt-*shell*-AuNR@*h*-SiO_2 was dramatically decreased (Figure 2d). Finite-element method (FEM)-based COMSOL simulation on a Pt-*shell*-AuNR model (2.2 nm thick Pt shell) estimated a drastic 9.2-fold decrease in the extinction at 785 nm and consequently in the electric field compared with that of a AuNR (Figure 2c and Tables S2 and S3), suggesting a nonradiative damping effect of the Pt shell. Using dark-field microscopy, we studied interparticle interactions of different NPs (AuNR@*h*-SiO_2, **Pt-*lam*-AuNR@***h*-SiO_2, and CTAB-AuNR dispersed in EG with Na_2PtCl_4). The light scattering intensities of AuNR@*h*-SiO_2 and **Pt-*lam*-AuNR@***h*-SiO_2 remained similar and consistent up to 30 min, but CTAB-AuNRs showed significant aggregation within 5 min (Figure 2e−g). This validated the key role of the *h*-SiO_2 confiner in maintaining sufficient interparticle separation and hindering any undesired plasmonic coupling due to NC aggregation.

We measured the electrochemically active surface area (ECSA) of different NPs (details are provided in SI section 2.27).[22] The estimated mass-normalized ECSA of **Pt-*lam*-AuNRs** (61.59 m^2/g) was found to be 4 times higher than that of Pt-*shell*-AuNRs (16.17 m^2/g) (Figure S31). In **M-*lam*-AuNR@***h*-SiO_2, the ultrathin M layer exposes a high number of catalytic metal sites, and the protective porous *h*-SiO_2 enclosure constructed a nanoreactor platform to carry out chemical reactions.[23] As a proof of application, we tested **Pt-*lam*-AuNR@***h*-SiO_2 for Pt-catalyzed conversion of nonfluorescent *N*-pentynoyl-protected rhodamine 110 (pro-Rh-110) (1 mg/mL in H_2O/DMSO) to green-fluorescent rhodamine 110 (Rh-110) with NIR laser irradiation (785 nm, 0.4 W/cm^2) at the bulk solution temperature (<40 °C) (Figure 3a).[24] The reaction resulted in the emergence of green fluorescence due to the production of free Rh-110 with >99% conversion (TOF = 0.53 min^{-1}) within 1 h (Figure 3b). Dark conditions did not result any measurable change in fluorescence at low temperatures (<40 °C), whereas raising the temperature of the reaction to 85 °C with an oil bath afforded ∼95% conversion within 1 h (Figure 3c). This result signified that the reaction can also be thermally induced at much higher temperatures. Under an identical laser flux, Pt-*shell*-AuNR@*h*-SiO_2 afforded ∼26 times slower conversion (TOF = 0.02 min^{-1}) relative to **Pt-*lam*-AuNR@***h*-SiO_2. Such a stark difference in reaction rates may be attributed to the suppressed LSPR extinction due

https://doi.org/10.1021/jacs.1c05753
J. Am. Chem. Soc. 2021, 143, 10582−10589

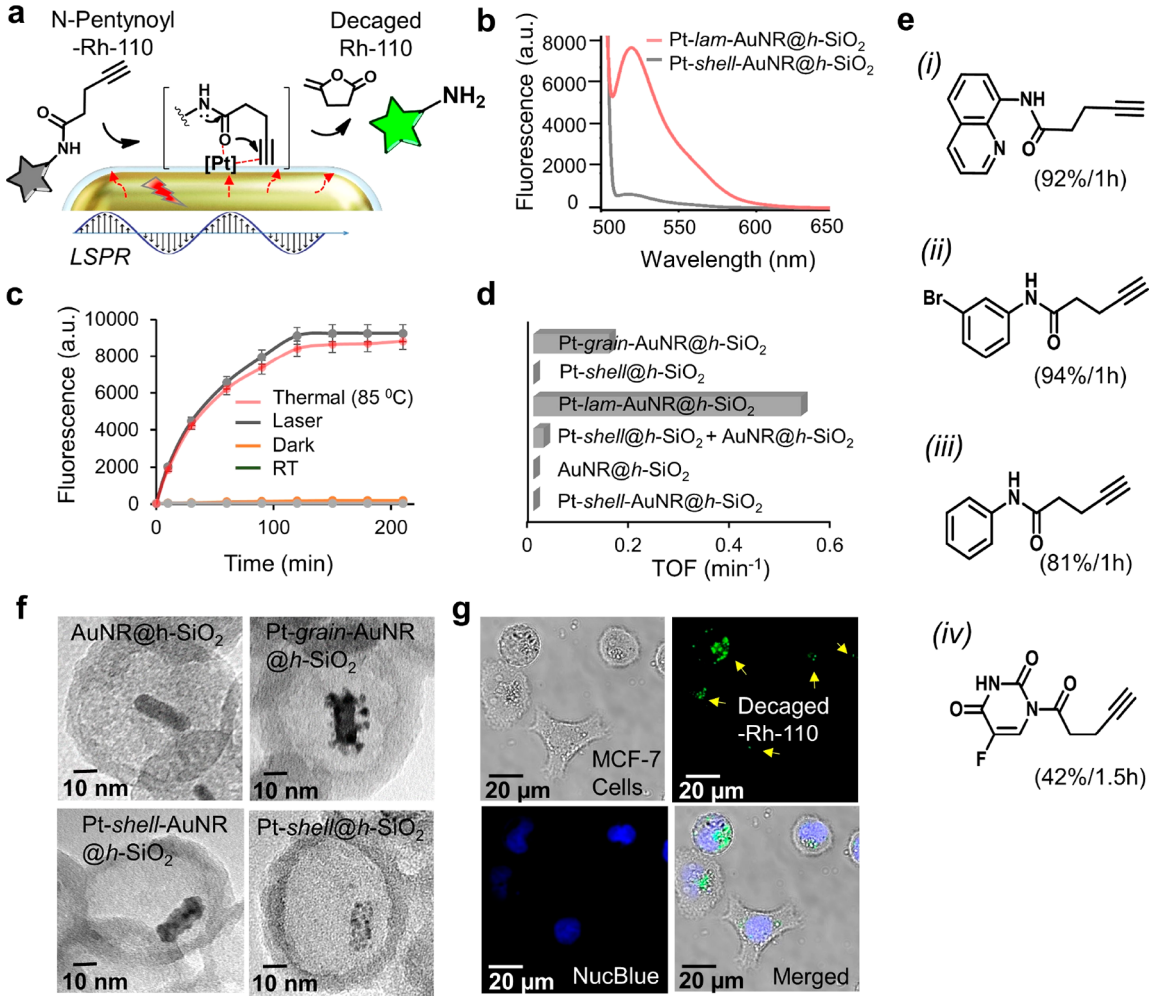

Figure 3. Catalytic properties of **Pt-*lam*-AuNR**@*h*-SiO_2 for decaging of *N*-pentynoyl-Rh-110. (a) Schematic of the Pt-catalyzed decaging reaction. (b) Fluorescence spectra for the reactions catalyzed by **Pt-*lam*-AuNR**@*h*-SiO_2 and Pt-*shell*-AuNR@*h*-SiO_2. (c) Time-dependent change in fluorescence of the reaction mixture under different conditions. (d) Comparison of TOF values for different catalysts. (e) Substrate scope for the catalytic reaction. (f) TEM images of different control catalysts. (g) Bright-field and fluorescence images showing intracellular catalysis in MCF-7 cells incubated with **Pt-*lam*-AuNR**@*h*-SiO_2.

to the thick Pt shell and consequently the weaker plasmon-induced effect in the case of Pt-*shell*-AuNR@*h*-SiO_2. Also, AuNR@*h*-SiO_2 showed no reactivity, validating the indispensable catalytic role of the outermost [Pt] layer.[24] In addition, Pt-*shell*@*h*-SiO_2 (without Au content) showed no reaction upon NIR irradiation (Figure 3d,f). These results deconvoluted the synergistic roles of the plasmonic and catalytic components, viz., the AuNR and ultrathin Pt layer, respectively. A mixture of AuNR@*h*-SiO_2 and Pt-*shell*@*h*-SiO_2 (having plasmonic and catalytic components in separate *h*-SiO_2 confiners) showed no reaction upon NIR irradiation, ruling out any interparticle energy transfer process and validating the fact that the plasmonic effect remained highly localized. Interestingly, Pt grains on AuNRs inside *h*-SiO_2 (Pt-*grain*-AuNR@*h*-SiO_2) showed a ca. 3.5 times lower reaction rate (TOF = 0.15 min^{-1}) than **Pt-*lam*-AuNR**@*h*-SiO_2 (Figure 3d,f), vindicating the intimate and extensively interfacial Pt lamination for efficient plasmonic energy flow to the surface Pt catalytic sites. The intimate fusion and adhesion of Pt atoms on the AuNR makes the catalytic surface in **Pt-*lam*-AuNR** highly robust, as was verified by the recyclability test using the same catalyst in multiple cycles (10 cycles) without any loss in activity (Figure S32). However, silica-free **Pt-*lam*-AuNRs** and Pt-*grain*-AuNRs showed reduced conversion yields of 68% and 14%, respectively (Figure S33), possibly due to NP-aggregation-mediated loss of catalytic activity. These experiments suggested an LSPR-induced catalytic mechanism in which plasmonic energy can be efficiently transferred to surface catalytic sites.[25] Under the CW laser irradiation (0.4 W/cm^2), the negligible photothermal temperature increase (Figure S17) is unlikely to increase the reaction rates.

To obtain supporting evidence for the involvement of charge carriers during catalysis, we performed the direct reduction of methylene blue (MB) to MB radical ion (MB_{red}) and affirmed efficient reaction in the case of **Pt-*lam*-AuNRs** (SI section 2.26 and Figure S34).[25a] We also investigated the generation and dynamics of hot charge carriers by transient absorption (TA) spectroscopy (SI section 2.19 and Figure S35).[26] The hot electron generation efficiency ($\Delta OD_{max}/OD$) of **Pt-*lam*-AuNRs** was found to be much higher than that of Pt-*shell*-AuNRs but slightly lower than that of AuNRs, and the excited charge carrier lifetime (τ) was found to be 2.94 ps, which was slightly lower than that of the AuNRs (3.8 ps). Evidently, the higher excited charge carrier generation efficiency and longer lifetime in the case of **Pt-*lam*-AuNRs** are critical for more efficient plasmonic energy flow, which in turn resulted in

https://doi.org/10.1021/jacs.1c05753
J. Am. Chem. Soc. 2021, 143, 10582−10589

higher catalytic efficacy (Figures 3e and S36−S40). Other LSPR-induced reactions such as Pd-catalyzed Suzuki−Miyaura and Heck C−C cross-couplings (Figure S41) and Pt-catalyzed reduction of nitroarenes (Figure S42) were also successfully carried out using **Pd-*lam*-AuNR**@*h*-SiO_2 and **Pt-*lam*-AuNR**@*h*-SiO_2, respectively (details are provided in SI sections 2.11 and 2.12).

The efficient LSPR-induced catalysis at physiological bulk temperature with remotely operable NIR light coupled with the biocompatibility, chemical inertness, and optical transparency of *h*-SiO_2 enclosure motivated us to utilize our nanoreactors for intracellular catalysis.[27] MCF-7 cells were incubated with **Pt-*lam*-AuNR**@*h*-SiO_2, followed by treatment with *N*-pentynoyl-Rh-110. Thereafter, upon NIR-light irradiation of the selected population of the cells, the emergence of green fluorescence was observed in the intracellular regions, confirming the generation of free Rh-110 (Figure 3g). Well-protected from the reach of large-sized complex biomolecules by *h*-SiO_2, the ultrathin Pt layer on the AuNRs not only helps to efficiently induce new-to-nature chemical reactions on demand with remotely operable nondamaging low laser powers but also minimizes the use of cytotoxic but catalytically versatile metals such as Pt.

In summary, we have devised a "confine and shine" strategy to modify ligand-free plasmonic NCs with atomically conformal layers of different noble transition metals by investing in LSPR-induced surface-centric and self-limited metal deposition chemistry. Our approach overcomes the bottlenecks of conventional metal growth methods, which are guided by complex reaction kinetic parameters, often resulting in heterogeneous and uncontrollable metal growth. Extensively useful LSPR-based properties remain well-preserved because of the ultrathin skinlike atomic lamination of nonplasmonic metals. The metal lamination process transforms the chemically inert Au surface into a highly functional catalytic platform that can be used to carry out a variety of light-induced chemical reactions with impressive TOFs. We have demonstrated the potential of our nanoreactor platform for bioorthogonal catalysis. Distinguished from the conventional nanomaterials synthesis approaches, our platform-based strategy provides inspiration to synergistically merge different paradigms of nanoscale properties, leading to applications in catalysis, sustainable energy conversion, biotechnology, and biomedical science.

■ ASSOCIATED CONTENT

Supporting Information

The Supporting Information is available free of charge at https://pubs.acs.org/doi/10.1021/jacs.1c05753.

Materials and methods, additional TEM images, XRD patterns, XPS spectra, NMR spectra, and simulation details (PDF)

■ AUTHOR INFORMATION

Corresponding Authors

In Su Lee − *Creative Research Initiative Center for Nanospace-Confined Chemical Reactions (NCCR) and Department of Chemistry, Pohang University of Science and Technology (POSTECH), Pohang 37673, Korea; Institute for Convergence Research and Education in Advanced Technology (I-CREATE), Yonsei University, Seoul 03722, Korea;* orcid.org/0000-0002-2588-1444; Email: insulee97@postech.ac.kr

Amit Kumar − *Creative Research Initiative Center for Nanospace-Confined Chemical Reactions (NCCR) and Department of Chemistry, Pohang University of Science and Technology (POSTECH), Pohang 37673, Korea;* orcid.org/0000-0001-7260-3044; Email: amitkumar@postech.ac.kr

Authors

Anubhab Acharya − *Creative Research Initiative Center for Nanospace-Confined Chemical Reactions (NCCR) and Department of Chemistry, Pohang University of Science and Technology (POSTECH), Pohang 37673, Korea*

Sateesh Dubbu − *Creative Research Initiative Center for Nanospace-Confined Chemical Reactions (NCCR) and Department of Chemistry, Pohang University of Science and Technology (POSTECH), Pohang 37673, Korea*

Sumit Kumar − *Center for Soft and Living Matter, Institute for Basic Science (IBS), and Department of Biomedical Engineering, School of Life Sciences, Ulsan National Institute of Science and Technology (UNIST), Ulsan 44919, Korea*

Nitee Kumari − *Creative Research Initiative Center for Nanospace-Confined Chemical Reactions (NCCR) and Department of Chemistry, Pohang University of Science and Technology (POSTECH), Pohang 37673, Korea*

Yeseul Kim − *Department of Mechanical Engineering, Pohang University of Science and Technology (POSTECH), Pohang 37673, Korea*

Sunae So − *Department of Mechanical Engineering, Pohang University of Science and Technology (POSTECH), Pohang 37673, Korea*

Taewan Kwon − *Creative Research Initiative Center for Nanospace-Confined Chemical Reactions (NCCR) and Department of Chemistry, Pohang University of Science and Technology (POSTECH), Pohang 37673, Korea*

Zhipeng Wang − *Department of Energy Science, Sungkyunkwan University (SKKU), Suwon 16419, Korea*

Junbeom Park − *Department of Chemistry, Pohang University of Science and Technology (POSTECH), Pohang 37673, Korea*

Yoon-Kyoung Cho − *Center for Soft and Living Matter, Institute for Basic Science (IBS), and Department of Biomedical Engineering, School of Life Sciences, Ulsan National Institute of Science and Technology (UNIST), Ulsan 44919, Korea;* orcid.org/0000-0001-6423-1834

Junsuk Rho − *Department of Mechanical Engineering and Department of Chemical Engineering, Pohang University of Science and Technology (POSTECH), Pohang 37673, Korea;* orcid.org/0000-0002-2179-2890

Sang Ho Oh − *Department of Energy Science, Sungkyunkwan University (SKKU), Suwon 16419, Korea*

Complete contact information is available at: https://pubs.acs.org/10.1021/jacs.1c05753

Notes

The authors declare no competing financial interest.

■ ACKNOWLEDGMENTS

This work was supported by the Basic Science Research Program through the National Research Foundation of Korea (NRF) funded by the Ministry of Science, ICT & Future

Planning (MSIP) (Grants NRF-2016R1A3B1907559 to I.S.L. and NRF-2020R1I1A1A01071721 to A.K.).

REFERENCES

(1) (a) Jiang, L.; Liu, K.; Hung, S.-F.; Zhou, L.; Qin, R.; Zhang, Q.; Liu, P.; Gu, L.; Chen, H. M.; Fu, G.; Zheng, N. Facet Engineering Accelerates Spillover Hydrogenation on Highly Diluted Metal Nanocatalysts. *Nat. Nanotechnol.* **2020**, *15*, 848−853. (b) Ghosh, S.; Roy, P.; Karmodak, N.; Jemmis, E. D.; Mugesh, G. Nanoisozymes: Crystal-Facet-Dependent Enzyme-Mimetic Activity of V_2O_5 Nanomaterials. *Angew. Chem., Int. Ed.* **2018**, *57*, 4510−4515.

(2) (a) Li, Z.; Jin, J.; Yang, F.; Song, N.; Yin, Y. Coupling Magnetic and Plasmonic Anisotropy in Hybrid Nanorods for Mechanochromic Responses. *Nat. Commun.* **2020**, *11*, 2883. (b) Xie, X.; Gao, N.; Deng, R.; Sun, Q.; Xu, Q.-H.; Liu, X. Mechanistic Investigation of Photon Upconversion in Nd^{3+}-Sensitized Core−Shell Nanoparticles. *J. Am. Chem. Soc.* **2013**, *135*, 12608−12611. (c) Kobayashi, H.; Yamauchi, M.; Kitagawa, H.; Kubota, Y.; Kato, K.; Takata, M. Hydrogen Absorption in the Core/Shell Interface of Pd/Pt Nanoparticles. *J. Am. Chem. Soc.* **2008**, *130*, 1818−1819.

(3) (a) Wang, G.; Huang, B.; Xiao, L.; Ren, Z.; Chen, H.; Wang, D.; Abruña, H. D.; Lu, J.; Zhuang, L. Pt Skin on AuCu Intermetallic Substrate: a Strategy to Maximize Pt Utilization for Fuel Cells. *J. Am. Chem. Soc.* **2014**, *136*, 9643−9649. (b) Henning, A. M.; Watt, J.; Miedziak, P. J.; Cheong, S.; Santonastaso, M.; Song, M.; Takeda, Y.; Kirkland, A. I.; Taylor, S. H.; Tilley, R. D. Gold−Palladium Core−Shell Nanocrystals with Size and Shape Control Optimized for Catalytic Performance. *Angew. Chem., Int. Ed.* **2013**, *52*, 1477−1480. (c) Wang, J. X.; Inada, H.; Wu, L.; Zhu, Y.; Choi, Y.; Liu, P.; Zhou, W.-P.; Adzic, R. R. Oxygen Reduction on Well-Defined Core−Shell Nanocatalysts: Particle Size, Facet, and Pt Shell Thickness Effects. *J. Am. Chem. Soc.* **2009**, *131*, 17298−17302. (d) Stamenkovic, V. R.; Mun, B. S.; Mayrhofer, K. J. J.; Ross, P. N.; Markovic, N. M. Effect of Surface Composition on Electronic Structure, Stability, and Electrocatalytic Properties of Pt-transition Metal Alloys: Pt-skin versus Pt-skeleton Surfaces. *J. Am. Chem. Soc.* **2006**, *128*, 8813−8819.

(4) (a) Sousa-Castillo, A.; Couceiro, J. R.; Tomás-Gamasa, M.; Mariño-López, A.; López, F.; Baaziz, W.; Ersen, O.; Comesaña-Hermo, M.; Mascareñas, J. L.; Correa-Duarte, M. A. Remote Activation of Hollow Nanoreactors for Heterogeneous Photocatalysis in Biorelevant Media. *Nano Lett.* **2020**, *20*, 7068−7076. (b) Zhou, L.; Swearer, D. F.; Zhang, C.; Robatjazi, H.; Zhao, H.; Henderson, L.; Dong, L.; Christopher, P.; Carter, E. A.; Nordlander, P.; Halas, N. J. Quantifying Hot Carrier and Thermal Contributions in Plasmonic Photocatalysis. *Science* **2018**, *362*, 69−72. (c) Aslam, U.; Chavez, S.; Linic, S. Controlling Energy Flow in Multimetallic Nanostructures for Plasmonic Catalysis. *Nat. Nanotechnol.* **2017**, *12*, 1000−1005.

(5) (a) Guo, J.; Zhang, Y.; Shi, L.; Zhu, Y.; Mideksa, M. F.; Hou, K.; Zhao, W.; Wang, D.; Zhao, M.; Zhang, X.; Lv, J.; Zhang, J.; Wang, X.; Tang, Z. Boosting Hot Electrons in Hetero-Superstructures for Plasmon-Enhanced Catalysis. *J. Am. Chem. Soc.* **2017**, *139*, 17964−17972. (b) Huang, H.; Zhang, L.; Lv, Z.; Long, R.; Zhang, C.; Lin, Y.; Wei, K.; Wang, C.; Chen, L.; Li, Z.-Y.; Zhang, Q.; Luo, Y.; Xiong, Y. Unraveling Surface Plasmon Decay in Core−Shell Nanostructures toward Broadband Light-Driven Catalytic Organic Synthesis. *J. Am. Chem. Soc.* **2016**, *138*, 6822−6828. (c) Grzelczak, M.; Pérez-Juste, J.; García de Abajo, F. J.; Liz-Marzán, L. M. Optical Properties of Platinum-Coated Gold Nanorods. *J. Phys. Chem. C* **2007**, *111*, 6183−6188. (d) Tan, S. F.; Bisht, G.; Anand, U.; Bosman, M.; Yong, X. E.; Mirsaidov, U. In Situ Kinetic and Thermodynamic Growth Control of Au−Pd Core−Shell Nanoparticles. *J. Am. Chem. Soc.* **2018**, *140*, 11680−11685. (e) Straney, P. J.; Diemler, N. A.; Smith, A. M.; Eddinger, Z. E.; Gilliam, M. S.; Millstone, J. E. Ligand-Mediated Deposition of Noble Metals at Nanoparticle Plasmonic Hotspots. *Langmuir* **2018**, *34*, 1084−1091. (f) Fennell, J.; He, D.; Tanyi, A. M.; Logsdail, A. J.; Johnston, R. L.; Li, Z. Y.; Horswell, S. L. A Selective Blocking Method to Control the Overgrowth of Pt on Au Nanorods. *J. Am. Chem. Soc.* **2013**, *135*, 6554−6561. (g) Zheng, H.; Smith, R. K.; Jun, Y.; Kisielowski, C.; Dahmen, U.; Alivisatos, A. P. Observation of Single Colloidal Platinum Nanocrystal Growth Trajectories. *Science* **2009**, *324*, 1309−1312.

(6) (a) Vara, M.; Roling, L. T.; Wang, X.; Elnabawy, A. O.; Hood, Z. D.; Chi, M.; Mavrikakis, M.; Xia, Y. Understanding the Thermal Stability of Palladium−Platinum Core−Shell Nanocrystals by In Situ Transmission Electron Microscopy and Density Functional Theory. *ACS Nano* **2017**, *11*, 4571−4581. (b) Guo, X.; Zhang, Q.; Sun, Y.; Zhao, Q.; Yang, J. Lateral Etching of Core−Shell Au@Metal Nanorods to Metal-Tipped Au Nanorods with Improved Catalytic Activity. *ACS Nano* **2012**, *6*, 1165−1175. (c) Ithurria, S.; Talapin, D. V. Colloidal Atomic Layer Deposition (c-ALD) Using Self-Limiting Reactions at Nanocrystal Surface Coupled to Phase Transfer between Polar and Nonpolar Media. *J. Am. Chem. Soc.* **2012**, *134*, 18585−18590. (d) Carino, E. V.; Crooks, R. M. Characterization of Pt@Cu Core@Shell Dendrimer-Encapsulated Nanoparticles Synthesized by Cu Underpotential Deposition. *Langmuir* **2011**, *27*, 4227−4235. (e) Mohamed, M. B.; Ismail, K. Z.; Link, S.; El-Sayed, M. A. Thermal Reshaping of Gold Nanorods in Micelles. *J. Phys. Chem. B* **1998**, *102*, 9370−9374.

(7) (a) Kamarudheen, R.; Kumari, G.; Baldi, A. Plasmon-Driven Synthesis of Individual Metal@semiconductor Core@shell Nanoparticles. *Nat. Commun.* **2020**, *11*, 3957. (b) Jin, R.; Charles Cao, Y.; Hao, E.; Métraux, G. S.; Schatz, G. C.; Mirkin, C. A. Controlling Anisotropic Nanoparticle Growth through Plasmon Excitation. *Nature* **2003**, *425*, 487−490.

(8) (a) Kumar, A.; Jeon, K.-W.; Kumari, N.; Lee, I. S. Spatially Confined Formation and Transformation of Nanocrystals within Nanometer-Sized Reaction Media. *Acc. Chem. Res.* **2018**, *51*, 2867−2879. (b) Wang, X.; Feng, J.; Bai, Y.; Zhang, Q.; Yin, Y. Synthesis, Properties, and Applications of Hollow Micro-/Nanostructures. *Chem. Rev.* **2016**, *116*, 10983−11060. (c) Li, Y.; Shi, J. Hollow−Structured Mesoporous Materials: Chemical Synthesis, Functionalization and Applications. *Adv. Mater.* **2014**, *26*, 3176−3205. (d) Lian, J.; Xu, Y.; Lin, M.; Chan, Y. Aqueous-Phase Reactions on Hollow Silica-Encapsulated Semiconductor Nanoheterostructures. *J. Am. Chem. Soc.* **2012**, *134*, 8754−8757.

(9) (a) Mackey, M. A.; Ali, M. R. K.; Austin, L. A.; Near, R. D.; El-Sayed, M. A. The Most Effective Gold Nanorod Size for Plasmonic Photothermal Therapy: Theory and In Vitro Experiments. *J. Phys. Chem. B* **2014**, *118* (5), 1319−1326. (b) Gole, A.; Murphy, C. J. Seed-Mediated Synthesis of Gold Nanorods: Role of the Size and Nature of the Seed. *Chem. Mater.* **2004**, *16*, 3633−3640.

(10) (a) Gorelikov, I.; Matsuura, N. Single-Step Coating of Mesoporous Silica on Cetyltrimethyl Ammonium Bromide-Capped Nanoparticles. *Nano Lett.* **2008**, *8*, 369−373. (b) Zhu, Z.; Zhang, S.; Li, C.; Zhang, J.; Yu, J.; Du, X.; He, L.; Zhang, X. A Mechanistic Study of Silica-Etching by Hot Water. *Phys. Chem. Chem. Phys.* **2018**, *20*, 1440−1446. (c) Wong, Y. J.; Zhu, L.; Teo, W. S.; Tan, Y. W.; Yang, Y.; Wang, C.; Chen, H. Revisiting the Stöber Method: Inhomogeneity in Silica Shells. *J. Am. Chem. Soc.* **2011**, *133*, 11422−11425. (d) Feng, J.; Wang, Z.; Shen, B.; Zhang, L.; Yang, X.; He, N. Effects of Template Removal on Both Morphology of Mesoporous Silica-Coated Gold Nanorod and Its Biomedical Application. *RSC Adv.* **2014**, *4*, 28683−28690.

(11) Zhang, S.; Zhang, L.; Liu, Z.; Liu, M.; Fan, Q.; Liu, K.; Gao, C. Robust Synthesis of Ultrathin Au−Ag Nanowires as a High-Surface-Area, Synergistic Substrate for Constructing Efficient Pt-Based Catalysts. *J. Mater. Chem. A* **2018**, *6*, 22161−22169.

(12) Kumar, A.; Kumar, S.; Rhim, W.-K.; Kim, G.-H.; Nam, J.-W. Oxidative Nanopeeling Chemistry-Based Synthesis and Photodynamic and Photothermal Therapeutic Applications of Plasmonic Core-Petal Nanostructures. *J. Am. Chem. Soc.* **2014**, *136*, 16317−16325.

(13) Forcherio, G. T.; Baker, D. R.; Boltersdorf, J.; Leff, A. C.; McClure, J. P.; Grew, K. N.; Lundgren, C. A. Targeted Deposition of Platinum onto Gold Nanorods by Plasmonic Hot Electrons. *J. Phys. Chem. C* **2018**, *122*, 28901−28909.

(14) Dong, H.; Chen, Y.-C.; Feldmann, C. Polyol Synthesis of NanoParticles: Status and Options Regarding Metals, Oxides,

https://doi.org/10.1021/jacs.1c05753
J. Am. Chem. Soc. 2021, 143, 10582−10589

Chalcogenides, and Non-metal Elements. *Green Chem.* **2015**, *17*, 4107−4132.
(15) (a) Yu, S.; Mohan, V.; Jain, P. K. Using Plasmonically Generated Carriers as Redox Equivalents. *MRS Bull.* **2020**, *45* (1), 43−48. (b) Kim, Y.; Smith, J. G.; Jain, P. K. Harvesting Multiple Electron−Hole Pairs Generated through Plasmonic Excitation of Au Nanoparticles. *Nat. Chem.* **2018**, *10* (7), 763−769.
(16) Fiévet, F.; Ammar-Merah, S.; Brayner, R.; Chau, F.; Giraud, M.; Mammeri, F.; Peron, J.; Piquemal, J.-Y.; Sicard, L.; Viau, G. The Polyol Process: A Unique Method for Easy Access to Metal Nanoparticles with Tailored Sizes, Shapes and Compositions. *Chem. Soc. Rev.* **2018**, *47*, 5187−5233.
(17) (a) Wilson, A. J.; Mohan, V.; Jain, P. K. Mechanistic Understanding of Plasmon-Enhanced Electrochemistry. *J. Phys. Chem. C* **2019**, *123*, 29360−29369. (b) Zhao, J.; Nguyen, S. C.; Ye, R.; Ye, B.; Weller, H.; Somorjai, G. A.; Alivisatos, A. P.; Toste, F. D. A Comparison of Photocatalytic Activities of Gold Nanoparticles Following Plasmonic and Interband Excitation and a Strategy for Harnessing Interband Hot Carriers for Solution Phase Photocatalysis. *ACS Cent. Sci.* **2017**, *3*, 482−488. (c) Yu, S.; Wilson, A. J.; Heo, J.; Jain, P. K. Plasmonic Control of Multi-Electron Transfer and C−C Coupling in Visible-Light-Driven CO_2 Reduction on Au Nanoparticles. *Nano Lett.* **2018**, *18*, 2189−2194.
(18) (a) Guo, W.; Johnston-Peck, A. C.; Zhang, Y.; Hu, Y.; Huang, J.; Wei, W. D. Cooperation of Hot Holes and Surface Adsorbates in Plasmon-Driven Anisotropic Growth of Gold Nanostars. *J. Am. Chem. Soc.* **2020**, *142*, 10921−10925. (b) Langille, M. R.; Personick, M. L.; Mirkin, C. A. Plasmon-Mediated Syntheses of Metallic Nanostructures. *Angew. Chem., Int. Ed.* **2013**, *52*, 13910−13940.
(19) (a) He, D. S.; Han, Y.; Fennell, J.; Horswell, S. L.; Li, Z. Y. Growth and Stability of Pt on Au Nanorods. *Appl. Phys. Lett.* **2012**, *101*, 113102. (b) Stolbov, S.; Zuluaga, S. Factors Controlling the Reactivity of Catalytically Active Monolayers on Metal Substrates. *J. Phys. Chem. Lett.* **2013**, *4*, 1537−1540.
(20) (a) Salmon, A. R.; Kleemann, M.-E.; Huang, J.; Deacon, W. M.; Carnegie, C.; Kamp, M.; de Nijs, B.; Demetriadou, A.; Baumberg, J. J. Light-Induced Coalescence of Plasmonic Dimers and Clusters. *ACS Nano* **2020**, *14*, 4982−4987. (b) Garnett, E. C.; Cai, W.; Cha, J. J.; Mahmood, F.; Connor, S. T.; Greyson Christoforo, M.; Cui, Y.; McGehee, M. D.; Brongersma, M. L. Self-Limited Plasmonic Welding of Silver Nanowire Junctions. *Nat. Mater.* **2012**, *11*, 241−249.
(21) Shimura, K.; Yoshida, H. Heterogeneous photocatalytic hydrogen production from water and biomass derivatives. *Energy Environ. Sci.* **2011**, *4*, 2467−2481.
(22) Wang, J.; Heo, J.; Chen, C.; Wilson, A. J.; Jain, P. K. Ammonia Oxidation Enhanced by Photopotential Generated by Plasmonic Excitation of a Bimetallic Electrocatalyst. *Angew. Chem., Int. Ed.* **2020**, *59*, 18430−18434.
(23) Prieto, G.; Tüysüz, H.; Duyckaerts, N.; Knossalla, J.; Wang, G.-H.; Schüth, F. Hollow Nano- and Microstructures as Catalysts. *Chem. Rev.* **2016**, *116*, 14056−14119.
(24) Abu Sohel, S. M.; Liu, R.-S. Carbocyclisation of Alkynes with External Nucleophiles Catalysed by Gold, Platinum and Other Electrophilic Metals. *Chem. Soc. Rev.* **2009**, *38*, 2269−2281.
(25) (a) Rao, V. G.; Aslam, U.; Linic, S. Chemical Requirement for Extracting Energetic Charge Carriers from Plasmonic Metal Nanoparticles to Perform Electron-Transfer Reactions. *J. Am. Chem. Soc.* **2019**, *141*, 643−647. (b) Aslam, U.; Chavez, S.; Linic, S. Controlling Energy Flow in Multimetallic Nanostructures for Plasmonic Catalysis. *Nat. Nanotechnol.* **2017**, *12*, 1000−1005. (c) Kale, M. J.; Christopher, P. Plasmons at the Interface. *Science* **2015**, *349*, 587−588.
(26) (a) Manjavacas, A.; Liu, J. G.; Kulkarni, V.; Nordlander, P. Plasmon-Induced Hot Carriers in Metallic Nanoparticles. *ACS Nano* **2014**, *8*, 7630−7638. (b) Guo, J.; Zhang, Y.; Shi, L.; Zhu, Y.; Mideksa, M. F.; Hou, K.; Zhao, W.; Wang, D.; Zhao, M.; Zhang, X.; Lv, J.; Zhang, J.; Wang, X.; Tang, Z. Boosting Hot Electrons in Hetero-Superstructures for Plasmon-Enhanced Catalysis. *J. Am. Chem. Soc.* **2017**, *139* (49), 17964−17972.
(27) (a) Lee, J.; Dubbu, S.; Kumari, N.; Kumar, A.; Lim, J.; Kim, S.; Lee, I. S. Magnetothermia-Induced Catalytic Hollow Nanoreactor for Bioorthogonal Organic Synthesis in Living Cells. *Nano Lett.* **2020**, *20*, 6981−6988. (b) Kumar, A.; Kumar, S.; Kumari, N.; Lee, S. H.; Han, J.; Michael, I. J.; Cho, Y.-K.; Lee, I. S. Plasmonically Coupled Nanoreactors for NIR-Light-Mediated Remote Stimulation of Catalysis in Living Cells. *ACS Catal.* **2019**, *9*, 977−990. (c) Destito, P.; Sousa-Castillo, A.; Couceiro, J. R.; López, F.; Correa-Duarte, M. A.; Mascareñas, J. L. Hollow Nanoreactors for Pd-Catalyzed Suzuki−Miyaura Coupling and *O*-Propargyl Cleavage Reactions in Biorelevant Aqueous Media. *Chem. Sci.* **2019**, *10*, 2598−2603.

https://doi.org/10.1021/jacs.1c05753
J. Am. Chem. Soc. 2021, 143, 10582−10589